

## NEAR FIELD TRAILING EDGE TONE NOISE COMPUTATION

Ching Y. Loh\*

Taitech Inc./NASA Glenn  
Cleveland, Ohio 44135, USA  
e-mail: fsloh@turbot.grc.nasa.gov

### Abstract

Blunt trailing edges in a flow often generate tone noise due to wall-jet shear layer and vortex shedding. In this paper, the space-time conservation element and solution element (CE/SE) method is employed to numerically study the near-field noise of blunt trailing edges. Two typical cases, namely, flow past a circular cylinder (aeolian noise problem) and flow past a flat plate of finite thickness are considered. The computed frequencies and the estimated sound pressure level (SPL) compare well with experimental data. For the aeolian noise problem, comparisons with the results of other numerical approaches are also presented.

### 1 Introduction

In today's aviation industry, everyday, thousands of commercial airliners take off and land at the airports around the world, accompanied by various uncomfortable noises, polluting the environment of the nearby areas. The noises due to airframe components, e.g. airfoil slat, landing gear and openings, etc. are one of the major noise sources. They are generated by the interaction of the vortex street in the turbulent wake. A blunt trailing edge often generates certain tone noise in the flow. Numerical investigations of airframe noise based on direct numerical simulation (DNS) need very fine grids and are hence expensive. Large eddy simulations (LES) allow a coarser grid since only large eddies are resolved and the smaller ones are modeled by a subgrid scale (SGS) model. Furthermore, some researchers use Reynolds averaged Navier-Stokes (RANS) methods to save more storage and CPU time [1-5].

In the present paper, we use a DNS type approach to investigate two benchmark noise problems, namely, the

noise generated by the flow past a circular cylinder (aeolian noise) and the noise generated by flow past a flat plate of finite thickness. Both may be categorized as blunt trailing edge noise. By 'DNS type', we mean that the grid may not be fine enough for the Kolmogorov scale of turbulence but is fine enough for the large turbulence structure (or large eddies) associated with the tone noise frequencies. This approach seems somewhat similar to LES but there is no explicit filtering or SGS model. More details are given later.

The space-time conservation element and solution element method (CE/SE) [6-8] is adopted for the computation. As demonstrated in our previous papers, the CE/SE scheme is well suited for aeroacoustics computation [9,10]. Because of the CE/SE non-reflecting boundary conditions (NRBC), which are based on *flux balance* [11], a smaller near field computational domain can be used in the present numerical simulation and helps to save both memory and CPU time.

The 2-D unstructured-grid Navier-Stokes (N-S) CE/SE scheme used here is briefly discussed in Section 2. Section 3 illustrates the initial and boundary conditions for these blunt trailing edge noise problems, in particular, the CE/SE NRBC. The numerical results are presented and compared to available experimental findings [12,15] in Section 4. Conclusions are drawn in Section 5.

### 2 The Numerical Scheme

The space-time conservation element and solution element (CE/SE) method is a low order (second order accurate in time and space) scheme with low dissipation. It is chosen in the present numerical investigation. A detailed description of the method can be found in [6-8]. In this Section, only a brief sketch of the scheme is given.

#### 2.1 Conservation Form of the 2-D Unsteady Compressible Navier-Stokes Equations

In general, the CE/SE method systematically solves a set of *integral* equations derived directly from the physical conservation laws and naturally captures shocks and other discontinuities in the flow. Both conservative variables and their derivatives are computed simultaneously

\*Taitech Inc., Member AIAA

as unknowns.

Consider a dimensionless conservation form of the unsteady 2-D Navier-Stokes equations of a perfect gas. Let  $\rho$ ,  $u$ ,  $v$ ,  $p$ , and  $\gamma$  be the density, streamwise velocity component, transverse velocity component, static pressure, and constant specific heat ratio, respectively. The 2-D Navier-Stokes equations then can be written in the following vector form:

$$\mathbf{U}_t + \mathbf{F}_x + \mathbf{G}_y = \mathbf{0}, \quad (1)$$

where  $x$ ,  $y$ , and  $t$  are the streamwise and transverse coordinates and time, respectively. The conservative flow variable vector  $\mathbf{U}$  and the flux vectors in the streamwise and radial directions,  $\mathbf{F}$  and  $\mathbf{G}$ , are given by:

$$\mathbf{U} = \begin{pmatrix} U_1 \\ U_2 \\ U_3 \\ U_4 \end{pmatrix}, \quad \mathbf{F} = \begin{pmatrix} F_1 \\ F_2 \\ F_3 \\ F_4 \end{pmatrix}, \quad \mathbf{G} = \begin{pmatrix} G_1 \\ G_2 \\ G_3 \\ G_4 \end{pmatrix},$$

with

$$U_1 = \rho, \quad U_2 = \rho u, \quad U_3 = \rho v, \\ U_4 = p/(\gamma - 1) + \rho(u^2 + v^2)/2.$$

The flux vectors are further split into inviscid and viscous fluxes:

$$\mathbf{F} = \mathbf{F}_i - \mathbf{F}_v, \quad \mathbf{G} = \mathbf{G}_i - \mathbf{G}_v,$$

where the inviscid fluxes are the same as in the Euler equations:

$$F_{i1} = U_2, \\ F_{i2} = (\gamma - 1)U_4 + [(3 - \gamma)U_2^2 - (\gamma - 1)U_3^2]/2U_1, \\ F_{i3} = U_2U_3/U_1, \\ F_{i4} = \gamma U_2U_4/U_1 - (\gamma - 1)U_2[U_2^2 + U_3^2]/2U_1^2, \\ G_{i1} = U_3, \quad G_{i2} = U_2U_3/U_1, \\ G_{i3} = (\gamma - 1)U_4 + [(3 - \gamma)U_3^2 - (\gamma - 1)U_2^2]/2U_1, \\ G_{i4} = \gamma U_3U_4/U_1 - (\gamma - 1)U_3[U_2^2 + U_3^2]/2U_1^2,$$

and the viscous fluxes are:

$$F_{v1} = 0, \quad F_{v2} = \mu(2u_x - \frac{2}{3}\nabla \cdot \mathbf{V}), \\ F_{v3} = \mu(v_x + u_y), \\ F_{v4} = \mu[2uu_x + (u_y + v_x)v - \frac{2}{3}(\nabla \cdot \mathbf{V})u + \\ \frac{\gamma}{Pr} \frac{\partial}{\partial y} (\frac{U_4}{U_1} - \frac{u^2 + v^2}{2})], \\ G_{v1} = 0, \quad G_{v2} = \mu(v_x + u_y), \\ G_{v3} = \mu(2v_y - \frac{2}{3}\nabla \cdot \mathbf{V}), \\ G_{v4} = \mu[2vv_y + (u_y + v_x)v - \frac{2}{3}(\nabla \cdot \mathbf{V})v +$$

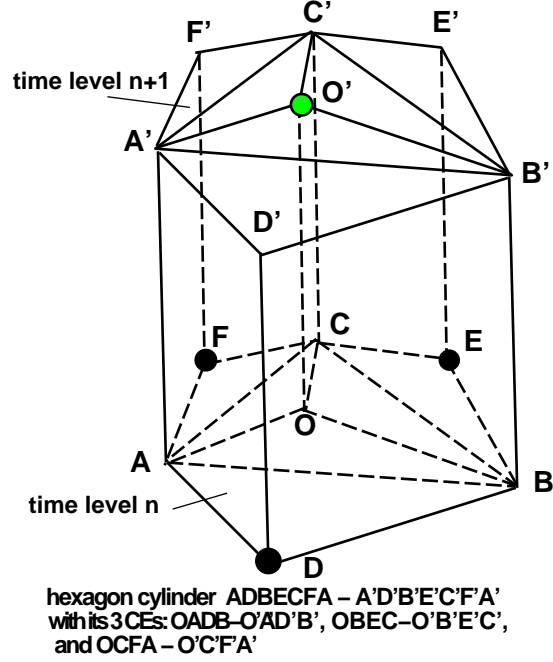


Figure 1: CE/SE unstructured grid in space-time  $E_3$  space.

$$\frac{\gamma}{Pr} \frac{\partial}{\partial y} (\frac{U_4}{U_1} - \frac{u^2 + v^2}{2})],$$

where  $u$ ,  $v$ ,  $u_x$ ,  $u_y$ ,  $v_x$ ,  $v_y$  are respectively the  $x$ - and  $y$ -flow velocity components and their derivatives, which can be written in terms of the conservative variables  $U_1, U_2, U_3$  and  $U_4$ , with  $Pr$  ( $= 0.72$ ) being the Prandtl number,  $\mu$  the viscosity, the velocity divergence

$$\nabla \cdot \mathbf{V} = u_x + v_y.$$

By considering  $(x, y, t)$  as coordinates of a three-dimensional Euclidean space,  $E_3$ , and using Gauss' divergence theorem, it follows that Eq. (1) is equivalent to the following integral conservation law:

$$\oint_{S(V)} \mathbf{H}_m \cdot d\mathbf{S} = 0, \quad \mathbf{m} = 1, 2, 3, 4, \quad (2)$$

where  $S(V)$  denotes the surface around a volume  $V$  in  $E_3$  and  $\mathbf{H}_m = (F_m, G_m, U_m)$ .

## 2.2 Unstructured Grid for CE/SE

The CE/SE scheme is constructed to take advantage of an unstructured triangle grid. The unstructured geometry used with the CE/SE scheme is illustrated in Fig. 1. Here,  $\triangle ABC$  is a typical triangle cell and  $D, E, F$  are the triangle centers of the neighboring cells. The flow variables at the previous time step are stored at the triangle cell centers. Three quadrilateral cylinders (conservation elements) are formed by the edges that connect the

vertices and the center of the triangle and its three neighbors. In the space-time  $E_3$  space, Eq. (2) is applied to the hexagon cylinder  $ADBE CF - A'D'B'E'C'F'$  of volume  $V$  that consists of these 3 quadrilateral cylinder  $CE$ s, see Fig 1.

In the CE/SE scheme, the above flux conservation relation, Eq. (2), in space-time is the *only* mechanism that transfers information between node points. A conservation element  $CE$  (here, quadrilateral cylinders) is the finite volume to which Eq. (2) is applied. Discontinuities are allowed to occur in a conservation element. A solution element  $SE$  associated with a grid node (e.g.,  $D$ ,  $E$ , or  $F$  in Fig. 1) is here a set of interface planes in  $E_3$  that passes through this node (e.g.  $DAA'D'$ ,  $DBB'D'$ ,  $EBB'E'$ ,  $ECC'E'$ , etc.). Each surface  $S(CE)$  is made up of segments belonging to *two* neighboring  $CE$ 's. Within a given solution element  $SE(j, n)$ , where  $j, n$  are the node index and time step, respectively, the flow variables are not only considered continuous but are also approximated by the linear Taylor series expansions. The surface flux can be calculated accurately and easily by first evaluating the flux vectors at the geometrical center of the surface through the above Taylor series expansions.

At time level  $n$ , the solution variables  $U$ ,  $U_x$ , and  $U_y$  are given at the three nodes  $D, E, F$  in Fig. 1 and  $U$ ,  $U_x$  and  $U_y$  at  $O'$  at the new time level  $n + 1$  are to be computed. In principle, each of the 3  $CE$ s provides 4 scalar equations when Eq. (2) is applied to the element. Hence, the 12 scalar equations needed for the 12 scalar unknowns at  $O'$  are available. All the unknowns are computed based on these relations. No extrapolations (interpolations) across a stencil of cells are needed.

More details about the unstructured CE/SE method can be found in [8].

### 3 The Trailing Edge Noise Problems

It is well known that when the trailing edge of a body is sharp, the turbulent wake generates broadband noise, while a blunt trailing edge produces certain tone noises due to the presence of wall-jets and the consequent large scale turbulence. Typical blunt trailing edges include, e.g., the flat plate of finite thickness and the circular cylinder. They are investigated separately in this section.

#### 3.1 The Aeolian Noise Problem

Aeolian noises, or the sounds generated by flow past a circular cylinder, are closely related to airframe noise and noise in automobiles, e.g. noise induced by auto-antenna. As it is important, the problem is chosen as one of the benchmark problems in CAA Workshop II [1].

Consider a Mach number  $M = 0.2$  uniform flow past a 2-D circular cylinder of diameter  $D = 1.9cm$ . Fig. 2 shows a sketch of the computational domain and the triangulated grid. As shown in the figure, the grid is ob-

tained by dividing a rectangular cell into 4 triangles. By so doing, the advantage is that the cell size, which is important in aeroacoustics computation, is well-controlled. The diameter  $D$  of the circular cylinder, the ambient speed of sound  $a_0$  and the ambient flow density are chosen as the scales of length, velocity and density respectively.

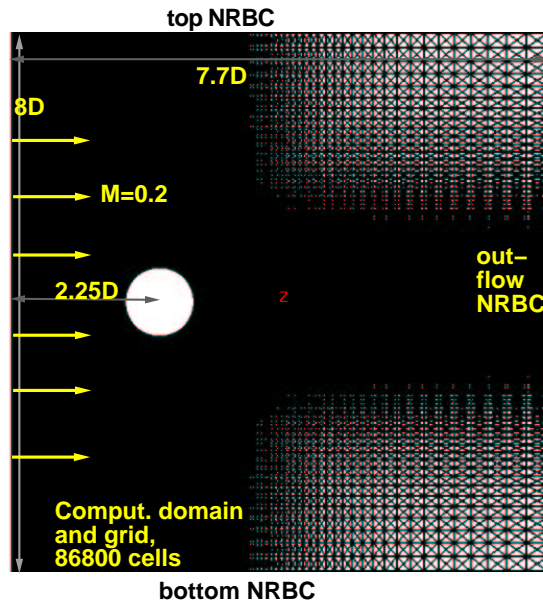


Figure 2: Geometry of the computational domain and unstructured grid,  $-2.1D \leq x \leq 5.5D$ ,  $-4D \leq y \leq 4D$ ; 7 exponentially growing rectangular cells (as sponge zones) at the top and bottom are not shown.

**3.1.1 Initial Conditions** Initially, the flow of the entire domain is set at the ambient conditions, i.e.,

$$\rho_0 = 1.0, \quad u_0 = 0, \quad v_0 = 0, \quad p_0 = 1/\gamma,$$

All spatial derivatives are set to zero.

**3.1.2 Non-Reflecting Boundary Condition (NRBC) for CE/SE** In the CE/SE scheme, NRBCs are constructed so as to allow fluxes from the interior domain to a boundary  $CE$  smoothly exit to the exterior of the domain. There are various variants of the NRBCs [9-11], the following are the ones employed in this paper.

For a grid node  $(j, n)$  lying at the outer border of the domain, where  $j$  is the grid node index number and  $n$  the time step, the Type I NRBC requires that

$$(U_x)_j^n = (U_y)_j^n = 0,$$

while  $U_j^n$  is kept fixed at the initially given steady boundary value. At the outflow boundary, where there are

substantial gradients in the radial direction, the Type II NRBC requires that

$$(U_x)_j^n = 0,$$

while  $U_j^n$  and  $(U_y)_j^n$  are now defined by simple extrapolation from the nearest interior node  $j'$ , *i.e.*,

$$U_j^n = U_{j'}^{n-1} \quad (U_y)_j^n = (U_y)_{j'}^{n-1}.$$

As will be observed later, these NRBCs are robust enough to allow a near field computation without disturbing or distorting the flow and acoustic fields.

**3.1.3 Boundary Conditions** At the inflow boundary, the flow variables are specified as the  $M = 0.2$  uniform flow:

$$\rho_i = 1.0, \quad u_i = 0.2, \quad v_i = 0, \quad p_i = 1/\gamma,$$

and their spatial derivatives are conveniently set to zero. Note that these inlet conditions also play a role as absorbing boundary conditions in the CE/SE scheme. At the surface of the circular cylinder, no-slip wall condition is applied. At the domain top and bottom Type I NRBC of the CE/SE method is used. The CE/SE outflow NRBC (Type II) is applied at the outflow boundary. Due to the inconsistency of the boundary conditions at the top, bottom and the inflow one, unpleasant non-physical gradients appear at the upper and lower left corners, although they do not propagate to the interior. To remove them, 7 rectangular cells with exponentially fast growth in size in the  $y$  direction are added to the top and bottom as ‘‘sponge zones’’. Each of these rectangular cells is then divided into 4 triangle cells as in the interior.

### 3.2 The Trailing Edge Tone Noise of a Flat Plate of Finite Thickness

In the case of a flat plate of finite thickness, due to flow separation, a wall-jet is formed downstream of the blunt trailing edge of the flat plate, tone noise is thus generated from the consequent Karman vortex street.

Consider a Mach number  $M = 0.3$  uniform flow past a 2-D flat plate of thickness  $D = 1''$  ( $2.54cm$ ). The flat plate extends into the computational domain with a length of  $3D$ . Fig. 3 shows a sketch of the computational domain. Similar to the previous problem, The plate thickness  $D$ , the ambient speed of sound  $a_0$  and the ambient flow density are used to scale length, velocity and density respectively. The domain shown in Fig. 3 is exactly the computational domain, no sponge zone is used for this problem. As in the previous problem, the ‘unstructured’ grid is obtained based on cutting a structured rectangular cell into 4 triangles.

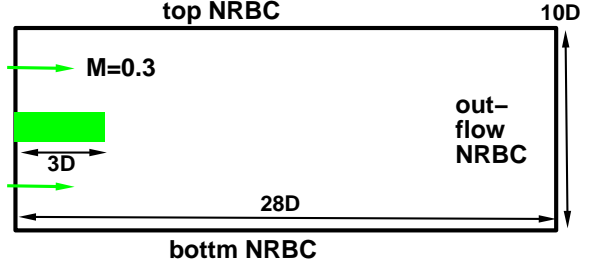


Figure 3: the computational domain for the flat plate noise problem; totally 77,600 triangular cells, no sponge zones.

**3.2.1 Initial Conditions** Initially, the flow of the entire domain is set at the ambient conditions, *i.e.*,

$$\rho_0 = 1.0, \quad u_0 = 0, \quad v_0 = 0, \quad p_0 = 1/\gamma,$$

All spatial derivatives are set to zero.

**3.2.2 Boundary Conditions** At the inflow boundary, the flow variables are specified as the  $M = 0.3$  uniform flow:

$$\rho_i = 1.0, \quad u_i = 0.3, \quad v_i = 0, \quad p_i = 1/\gamma,$$

and their spatial derivatives are conveniently set to zero. The no-slip wall boundary condition is applied to the flat plate. The top, bottom and outflow NRBC are the same as the previous problem, but no sponge zones are used.

## 4 Numerical Results

In this section, numerical results for both the aeolian and flat plate trailing edge noises are presented and compared to their respective experimental data and results by other numerical approaches when they are available.

### 4.1 Aeolian Noise Problem

In order to have a sizable sampling time series for FFT (fast Fourier transform) analysis, with non-dimensional time step size  $\Delta t = .005$ , over half million time steps are run. Fig. 4 - Fig. 6 demonstrate the isobars or numerical Schlierens at time step 410,000 and 545,000. The unsteadiness and the Karman vortex street in the wake are clearly displayed. A point located at  $(0D, 3.25D)$  (Fig. 4) is selected for recording the time series. At this location, there is no direct influence from the Karman vortex street. Fig. 7 illustrates the non-dimensional pressure history at this point. Fig. 8 depicts the result of FFT, *i.e.*, the sound pressure level (SPL) vs. frequency at this selected location. The SPL is based on the relative level to  $20 \mu Pa$ .

**4.1.1 Tone noise frequency** At Reynolds number  $Re = 90,000$  the highest peak of SPL in the plot corresponds to a computed frequency of 617 Hz

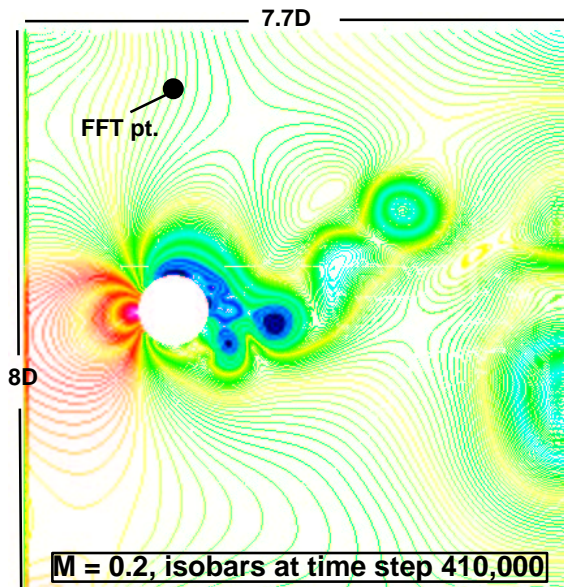


Figure 4: Instantaneous isobars at time step 410,000.

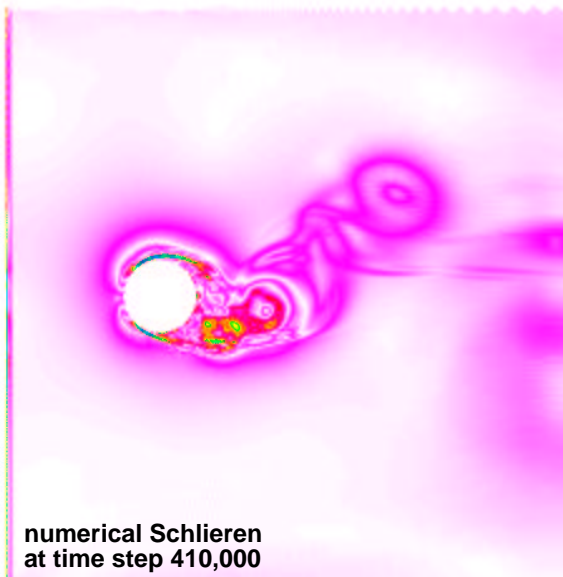


Figure 5: Instantaneous numerical Schlierens at time step 410,000.

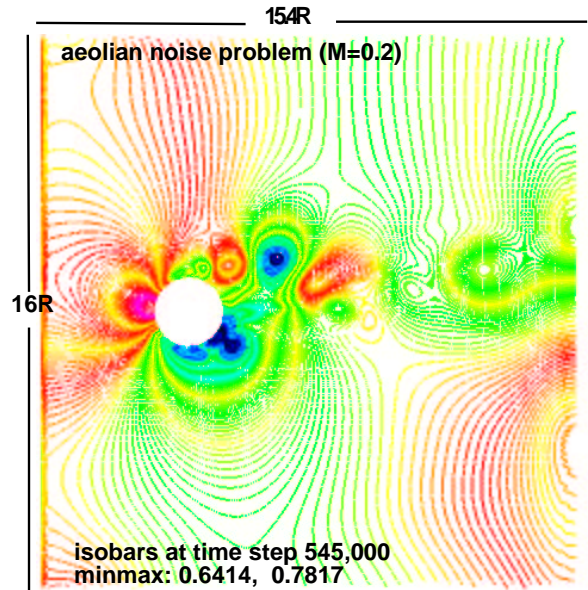


Figure 6: Instantaneous isobars at time step 545,000.

(with a  $3db$  ‘bandwidth’ or binwidth of 88 Hz), which is quite close to the experimental one of 643 Hz [1] at this  $M = 0.2$  Mach number, despite the crude resolution in frequency. A numerical experiment with a “very high” Reynolds number is also tested. The computed frequency is 652 Hz, slightly higher but still within a 4% range of the experimental 643 Hz. The phenomenon that the frequency ( or Strouhal number) around this range of Reynolds number does not significantly change with  $Re$  is justified by experimental observation (see Schlichting [13]). and also agrees with Townsend’s observation [14] that the large scale turbulence only weakly depends on the Reynolds number. The term “very high” used here is a synonym of turning off the viscous terms in the scheme. As a result of the numerical damping in the scheme, viscous effects still exist. According to the chart in Schlichting’s book (p.32, [13] ), we speculate that the effective  $Re$  is probably in the order of  $O(10^4)$  to  $O(10^5)$ .

It is interesting to compare the computed frequency with the results by other numerical approaches from the CAA Workshop II [12].

Table 1 lists the computed frequencies by several other researchers [2 - 5]. Generally, they use either compressible (Comp.) or incompressible (Incomp.) flow solver with RANS (Reynolds averaged Navier-Stokes), LES, or DNS and then an acoustic solver is applied. It is observed that, compared to the experimental result of 643 Hz, there is an error varying from 10 – 60%, while for  $Re$  from 90,000 to  $O(10^5)$ , the current method yields a error within only 4%, and no acoustic solver is employed at all.

Table 1: comparison of computed frequencies

Experiment	Brentner <i>et al</i>	Kumarasamy <i>et al</i>	Pope	Spyropoulos and Holmes	CE/SE
643 Hz.	815-1031	710	753	550	617 652
Flow Solver	Comp. RANS	Incomp. RANS	Incomp. DNS	Incomp. LES	Comp. DNS
Acoustic Solver	FW-H	Helmholtz	A/VS	Curle	none
Re	1k-90k	90k	20k	90k	90k  very high

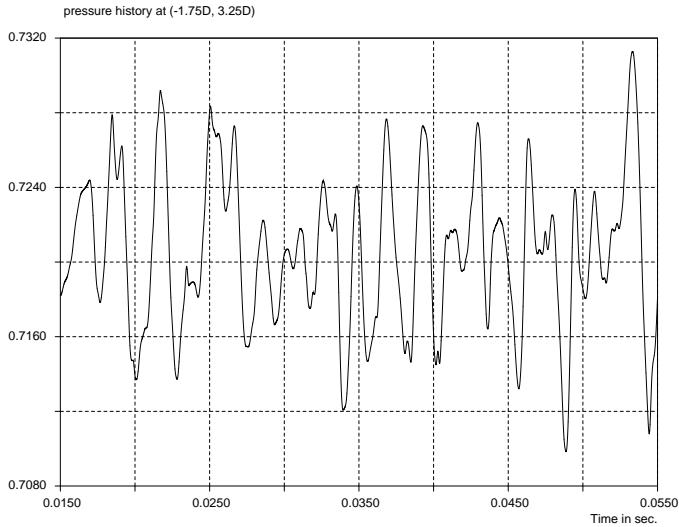


Figure 7: History of pressure fluctuation at the FFT point (recorded every 20 time steps).

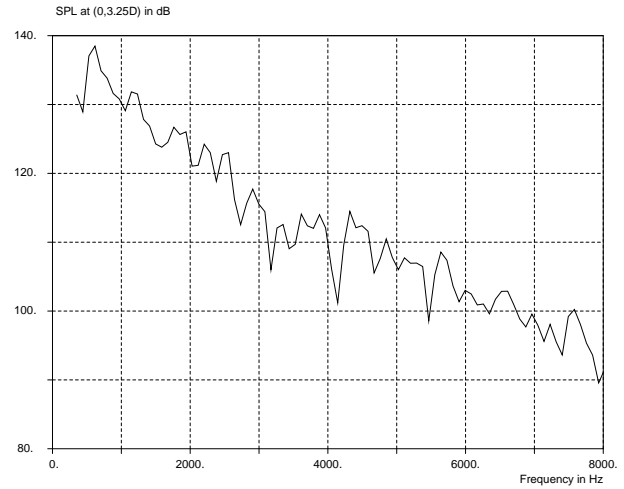


Figure 8: Sound pressure Level for Re=90,000 at (0, 3.25D), the highest peak corresponds to 617 Hz and 138 dB.

#### 4.1.2 Sound pressure level of the tone noise

Since the computation is two-dimensional, and the computational domain is in the near field (within 8 diameters), there is no direct comparison of the sound pressure level (SPL) to the experimental data which is of 3-D nature and measured at a location 35 diameters away from the circular cylinder center [12]. However, after some approximation and simple analysis from the first principle, an estimated SPL for 3-D flow SPL at  $r_0 = 35D$  in the direction of  $90^\circ$  can be obtained.

Based on the 2-D computation as shown in Fig. 8, at a point of (0D, 3.25D) (see the ‘FFT point’ in Fig. 4) which is in the  $90^\circ$  direction with  $x$  axis, the SPL is 138.5 dB. If the noise source is regarded to be a simple one and locates approximately at the circular cylinder centerline, for 2-D flow, the SPL attenuation is inversely proportional to  $r^2$ , where  $r$  is the distance from the source to the measuring point. Therefore, at the point  $Q$  (0, 35D) in the  $90^\circ$  direction the SPL is estimated to be:

$$SPL_{2d} = 138 - 20\log(35D/3.25D) = 117.9dB.$$

This result is obtained under the 2-D assumption that the circular cylinder is infinitely long.

According to the experiment [3, 12], a cylinder length of 10D is used.  $Q$  is assumed at the mid-plane normal to the cylinder centerline (the  $z$  direction), the cylinder rod ranges from  $z = -5D$  to  $z = 5D$ . For truly 3-D flow, let  $p(z)$  be the r.m.s. pressure contribution from a line segment  $dz$  at  $z$  (along the cylinder centerline) to  $Q$ . Then

$$p(z) = \frac{r_0^2}{r_0^2 + z^2} p_0, \quad p_0 = p(0).$$

Generally, let  $L$  be the half length of the cylinder, the square of the total sound pressure at  $Q$  is

$$p^2_L = \int_{-L}^L p_0^2 \frac{dz}{[1 + (z/r_0)^2]^2} = r_0 p_0^2 [\alpha_0 + 0.5 \sin(2\alpha_0)],$$

where  $\alpha_0 = \tan^{-1}(L/r_0)$ . Let  $L = 5D$  and  $L = \infty$  respectively and the ratio

$$R = \frac{p^2_{5D}}{p^2_{\infty}} = 0.1794612$$

Therefore, the sound pressure level at  $Q$  is estimated as:

$$SPL_{3d} = SPL_{2d} + 10\log R = 110.4dB$$

Table 2 lists the numerical SPLs at these two locations at an angle of  $90^\circ$  and comparison to the experimental data. Recall that the basic computation is a two dimensional one, while the experimental data is for a circular cylinder of finite length in 3-D space, the agreement is excellent.

Table 2: SPL of aeolian tone noise at  $90^\circ$  angle

r (distance)	Experiment [12]	CE/SE numerical
3.25D		138.5 dB
35D	111 dB	110.4 dB (estimated)

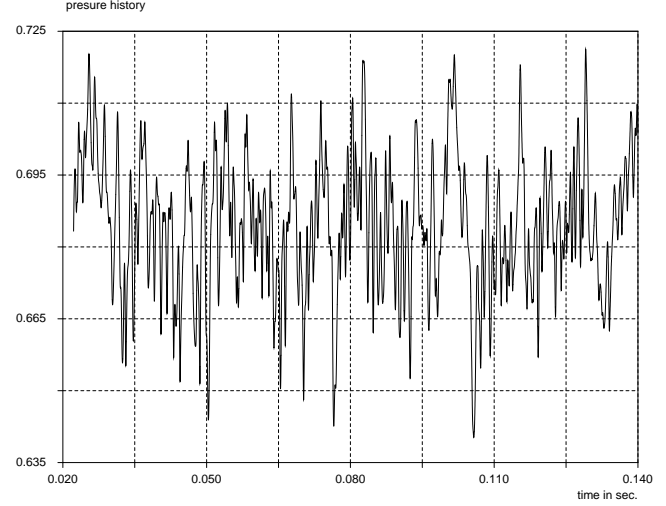


Figure 10: Pressure history at the FFT point (recorded at every 2 time steps).

#### 4.2 Trailing Edge Noise Tone of a flat Plate

With non-dimensional time step size  $\Delta t = .005$ , 390,000 time steps are run. Fig. 9 demonstrates the instantaneous isobars at the last time step. The unsymmetric unsteadiness and the Karman vortex street in the wake are evident. Since there is no sponge zone, the ‘matching layer’ between the steady Type I NRBC at the top and bottom boundaries are observed. Also, at the upper and lower left corners, non-physical gradients due to inconsistency of inflow boundary condition and the Type I NRBCs are present. However, they have practical no influence on the interior flow. A point located at  $(1.5D, 3D)$  is selected for recording the time series. At this location, there is no direct influence from the Karman vortex street. Fig. 10 illustrates the non-dimensional pressure history at this point. Fig. 11 depicts the PSD vs. frequency at this selected location and the experimental results by Heinemann *et al* [15] for similar cases. The Reynolds number is in the magnitude of  $10^4$  to  $10^5$  (“very high”). The highest peak of PSD in the plot corresponds to a computed frequency of 791 Hz (with a 3db binwidth 33 Hz). Experimentally, from Heinemann’s chart in Fig. 11, for Mach number  $M = 0.3$ , the corresponding Strouhal number  $S = 0.195$ . Assuming  $D = 2.54cm$  and speed of sound equal to  $343m/s$ , it is equivalent to 790 Hz,

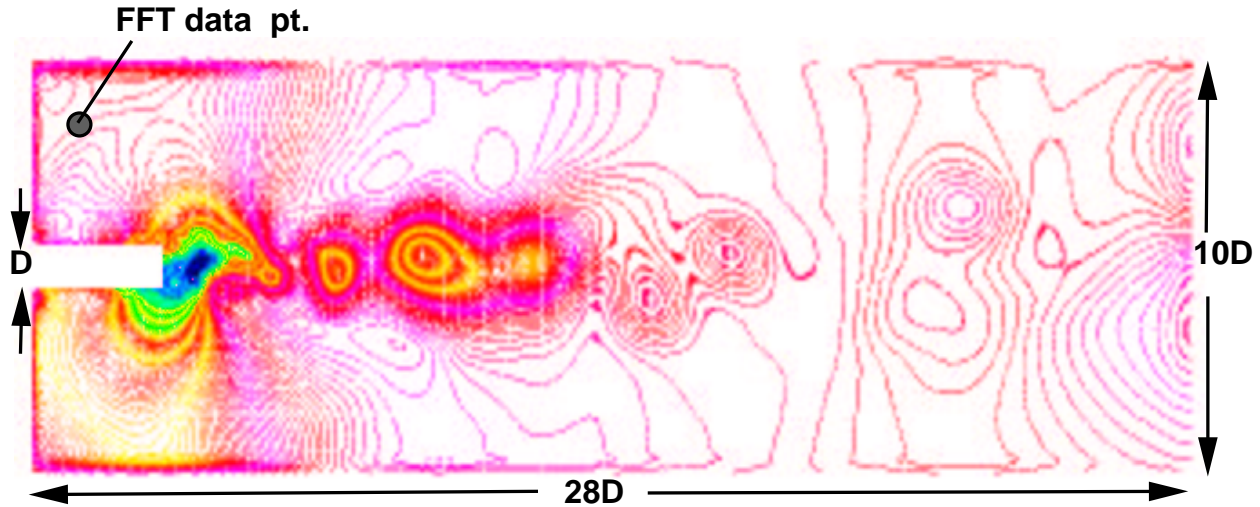


Figure 9: Instantaneous isobars at time step 390,000, for flow past the flat plate.

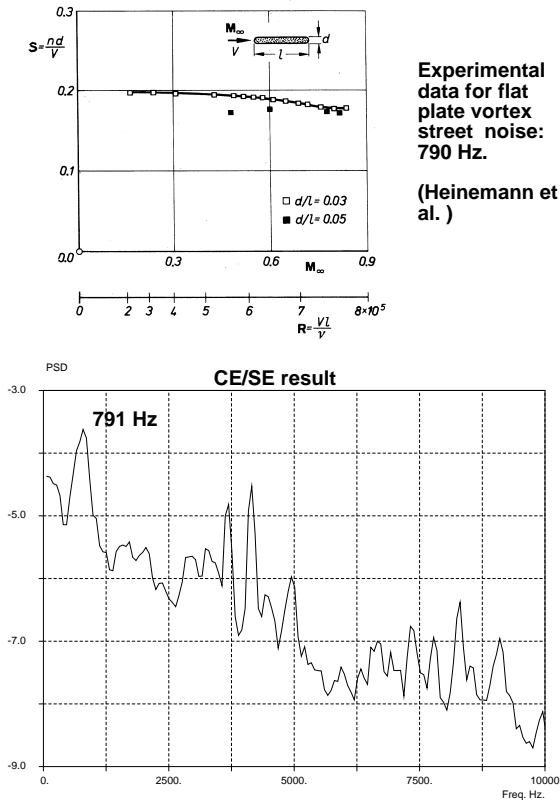


Figure 11: PSD and experimental data.

Table 3: **Flate plate tone noise frequency**

Experiment (Heinemann <i>et al</i> )	CE/SE numerical
790 Hz.	791 Hz

almost identical to the computed value, as shown in Table 3. No SPL data is collected since there is no experimental data in [15] to compare with.

## 5 Concluding Remarks

In this paper, a DNS type numerical approach is adopted to simulate the trailing edge tone noises arising from large scale turbulence. Good results in frequency and SPL are obtained and compare favorably to the experimental ones and the results by other numerical approaches.

In the DNS type approach, we attempt to simulate only the large scale turbulence, which is believed to be the tone noise generating source. The smaller scale turbulences (higher frequencies and wave numbers) are practically ignored without a subgrid scale model, since we are interested mostly in the aeroacoustic data. The CE/SE is a scheme of conservation laws. When the divergence theorem (2) is applied to find the cell average, it also plays a role as a filter ( such as the one in LES approach). High frequency and high wave number disturbances are filtered out and aliasing errors are unlikely to occur.

The novel NRBC based on flux balance is simple and

genuinely multi-dimensional. It allows the use of a small computational domain in the noise computation.

### Acknowledgements

This work received support from the Supersonic Propulsion Technology Project Office of NASA Glenn Research Center. The author is grateful to Dr. Richard A. Blech and Dr. James Scott for carefully reviewing the paper.

### References

- [1] C.K.W.Tam, J.C.Hardin, Eds., "Second Computational Aeroacoustics (CAA) Workshop on Benchmark problems", NASA CP-3352, June,1997.
- [2] K.S.Brentner, J.S.Cox, C.L.Rumsey and B.A.Younis, 'Computation of Sound generated by Flow over a Circular Cylinder: an Acoustic Analogy Approach', in "Second Computational Aeroacoustics (CAA) Workshop on Benchmark problems", NASA CP-3352, June,1997. C.K.W.Tam and J.C.Hardin, Eds.
- [3] S.Kumarasamy, R.A.Korpus J.B.Barlow, 'Computation of Noise due to the Flow over a Circular Cylinder', in "Second Computational Aeroacoustics (CAA) Workshop on Benchmark problems", NASA CP-3352, June,1997. C.K.W.Tam and J.C.Hardin, Eds.
- [4] D.S.Pope, 'A Viscous/Acoustic Splitting Technique for Aeolian Tone prediction', in "Second Computational Aeroacoustics (CAA) Workshop on Benchmark problems", NASA CP-3352, June,1997. C.K.W.Tam, J.C.Hardin, Eds.
- [5] E.T.Spyropoulos and B.S.Holmes, 'Large-Eddy of a High Reynolds Number Flow Around a Cylinder Including Aeroacoustic prediction' in "Second Computational Aeroacoustics (CAA) Workshop on Benchmark problems", NASA CP-3352, June,1997. C.K.W.Tam and J.C.Hardin, Eds.
- [6] Chang, S. C., "The Method of Space-Time Conservation Element and Solution Element—A New Approach for Solving the Navier-Stokes and Euler Equations," *Journal of Computational Physics*. vol. 119, pp. 295-324 (1995).
- [7] Chang, S.-C., Wang, X.-Y. and Chow, C.-Y., "The Space-Time Conservation Element and Solution Element Method—A New High Resolution and Genuinely Multidimensional Paradigm for Solving Conservation Laws," *J. Comp. Phys.* vol. 159, pp. 89-136 (1999).
- [8] Wang, X.-Y. and Chang S.-C., "A 2-D Non-splitting Unstructured Triangular Mesh Euler Solver Based on the Space-Time Conservation Element and Solution Element Method" *C.F.D. J.* vol. 8, pp309-325 (1999).
- [9] Loh, C. Y., Hultgren, L. S. and Chang S.-C., "Computing Waves in Compressible Flow Using the Space-Time Conservation Element Solution Element Method," *AIAA J.*, Vol. 39, pp. 794-801 (2001).
- [10] Loh, C. Y., Hultgren, L. S., Chang, S.-C. and Jorgenson, P. C. E., "Vortex Dynamics Simulation in Aeroacoustics by the Space-Time Conservation Element Solution Element Method," *AIAA Paper 99-0359* (1999).
- [11] Loh, C. Y., Hultgren, L. S., and Jorgenson, P. C. E., 'Near Field Screech Noise Computation for an Underexpanded Supersonic Jet by the CE/SE Method', *AIAA Paper 2001-2252*, (2001).
- [12] J.C. Hardin, 'Solution Comparisons: Category 4', in "Second Computational Aeroacoustics (CAA) Workshop on Benchmark problems", NASA CP-3352, June,1997. C.K.W.Tam and J.C.Hardin, Eds.
- [13] H.Schlichting, 'Boundary-Layer Theory', McGraw Hill, 1979.
- [14] A.A.Townsend, 'The Structure of turbulent Shear Flow', 2nd edition, Cambridge University Press, 1976.
- [15] H.J.Heinemann, O.Lawaczeck and K.A.Buterfisch, 'Karman vortices and their Frequency Determination in the Wakes of Profiles in the Sub-and Transonic Regime', *Sumposium Transonicum II*, Goettingen, Germany, Sept. 1975; Springer-Verlag 1976, pp. 75-82.